

# Hydrogel Ionotronics with Ultra-Low Impedance and High Signal Fidelity across Broad Frequency and Temperature Ranges

Bowen Yao, Shuwang Wu, Ruoxing Wang, Yichen Yan, Anne Cardenas, Dong Wu, Yousif Alsaied, Wenzhuo Wu, Xinyuan Zhu, and Ximin He\*

**Ionotronics, emerging devices that couple gel ionic conductors and electronic circuits, have shown great promise as stretchable alternatives with multi-functionalities to conventional rigid devices, ranging from energy harvesting to sensing, displaying, and actuation. However, current hydrogel ionotronics' performances are still unsatisfactory: i) upon high alternating current frequency (> 1000 Hz), the ionic conductivity dominates but is rather low and drops further drastically as temperature decreases; ii) upon low frequency (< 1000 Hz), the unstable and high impedance at the electrode/hydrogel interface dominates unfavorably but has been overlooked previously. To remedy these issues, herein, a systematic strategy is proposed by employing a highly ionically-conductive anti-freezing hydrogel and electronically-conductive porous polymer films with high electrical-double-layer capacitance as electrodes to connect the hydrogel and metal leads. The hydrogel has an ultra-high conductivity, while being transparent, stretchable, and easily prepared by one-step photogelation. Meanwhile, the conducting polymer electrodes realize a stable and low interfacial impedance and improved voltage tolerance, enabling much higher fidelity of ion-electron signal transduction than using gold electrodes. This strategy can be applied to construct various ionotronics for broad applications, including triboelectric nanogenerators, touch panels, displays, soft robotics, and multifunctional electronics with broad operational frequency and temperature ranges.**

## 1. Introduction

Stretchable electronics represents a promising emerging field, opening up enormous opportunities in energy harvesting and storage,<sup>[1]</sup> displays,<sup>[2,3]</sup> sensors,<sup>[4]</sup> and soft robotics.<sup>[5,6]</sup> Particularly, ionotronics based on electrolyte-loaded hydrogels as conductors,<sup>[7,8]</sup> a novel ionic analog of conventional electronics, can imitate the signal transmittance in living matter, with tissue-like ionic conductance, softness, and stretchability. Their additional merits of being transparent, mechanically tunable, and stimuli-responsive reveal enormous potential in structural design and rational control of properties to cater to various human-machine interfaces. The examples range from basic ionotronic elements (e.g., ionic conductors, transistors, and logic gates),<sup>[9]</sup> electromechanical transduction,<sup>[10]</sup> energy harvesting devices (triboelectricity,<sup>[11,12]</sup> ionic concentration gradient generator,<sup>[13]</sup> or thermoelectric generator<sup>[14]</sup>) to optically transparent multifunctional devices such as electroluminescence<sup>[15]</sup> and touch sensing<sup>[16]</sup> for human-machine interactions.

However, their electrical performance and the reliability at a low-frequency AC were not addressed and became worse at low temperatures. Low-frequency AC is a common operating scenario for many ionotronic devices.<sup>[7,8]</sup> For example, 1) by using ionic hydrogels as conductors, low-impedance ionotronics, such as the one loaded with a light-emitter diode (LED), unavoidably demand a highly complicated program to control their brightness determined by both input voltage and voltage change rate, rather than by voltage only as in conventional pure electronic systems. 2) If a high-impedance device is loaded in the ionotronics, such as dielectric-elastomer-based devices, the voltage tolerance, and electrical stability are also limited, as electrochemical side-reactions are easily triggered at the electrode/hydrogel interface. 3) For digital signal-communication, current ionotronic devices usually exhibit a poorer transaction quality than its pure electronic counterpart, being interfered by the unstable electrode/hydrogel interface. Thus, broad frequency, voltage, and working temperature

B. Yao, S. Wu, R. Wang, Y. Yan, A. Cardenas, D. Wu, Y. Alsaied, X. He  
Department of Materials Science and Engineering  
University of California  
Los Angeles, CA 90095, USA  
E-mail: ximinhe@ucla.edu

B. Yao, S. Wu, X. Zhu  
School of Chemistry and Chemical Engineering  
State Key Laboratory of Metal Matrix Composites  
Shanghai Jiao Tong University  
Shanghai 200240, China

R. Wang, W. Wu  
School of Industrial Engineering  
Purdue University  
West Lafayette, IN 47907, USA

 The ORCID identification number(s) for the author(s) of this article can be found under <https://doi.org/10.1002/adfm.202109506>.

DOI: 10.1002/adfm.202109506

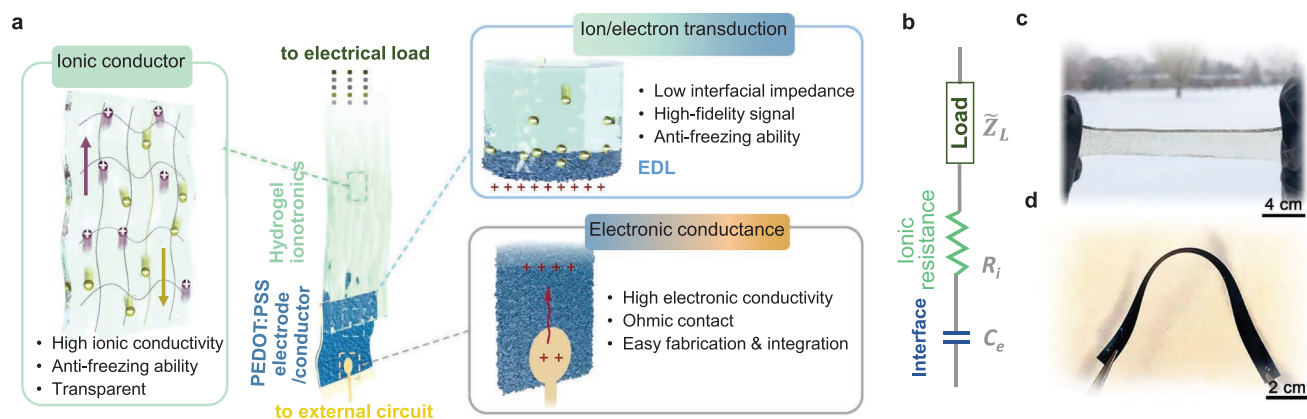


**Figure 1.** a) Schematics of antifreezing ionotronics. The ionotronics consist of three parts: using an electronically conductive polymer as the electrode and conductive lead to connect device-loaded ionically conductive hydrogel to external circuits for improved ion/electron transduction with a low interfacial impedance and high signal fidelity. b) Simplified equivalent circuit of the hydrogel ionotronics, where  $C_e$ ,  $R_i$ , and  $\tilde{Z}_L$  represent the capacitance of the electrode, ionic resistance of hydrogel, and the impedance of the electrical loads, respectively. c) Digital photograph of the antifreezing, conductive, transparent, and stretchable PAAm/ $H_2SO_4$  hydrogel stretched by hands for three times of original length, remaining unfrozen and stretchable outdoor in cold weather. d) Digital photograph of the PEDOT:PSS electrode showing its good flexibility.

ranges are highly desirable for the reliable performance of hydrogel ionotronics.

In principle, high-performance hydrogel ionotronics demand: i) high ionic conductance within the ionic conductor and ii) good transduction between ions and electrons at the ionic-conductor/electrode interface, that is, a low interfacial impedance, via non-faradic (formation of an electrical double layer, EDL) or faradic (electrochemical reactions) processes (Figure 1a, 1b). Between the two critical factors, the former usually dominates the electrical behaviors of ionotronics upon an alternating current (AC) of high frequency ( $> 1000$  Hz), while the latter becomes dominant upon low frequency as it determines the overall impedance, stability, signal fidelity, and voltage tolerance of the ionotronics. Most current hydrogel ionotronic devices employ metals (such as gold) as electrodes to transduce the electronic and ionic signals.<sup>[7,10,13]</sup> In this study, we have found that traditional hydrogel/metal-based ionotronics exhibit a 1500-fold increase in impedance as the frequency of the input signal decreases from  $10^5$  to 0.1 Hz. Both the impedance and phase angle also vary with the input voltage, which leads to serious distortion of the AC waveform even at voltages as low as 0.1 V. Therefore, these issues have severely impacted the overall device performance and reliability especially at a low-frequency AC ( $< 100$  Hz) as discussed above.

Although the electrochemical behaviors at the ionic-conductor/electrode interfaces have drawn considerable attention in other electronics such as supercapacitors and bioelectronics, which share the same basic science of ion-electron interconversions, hydrogel ionotronics focus more on signal transduction and transmission, processability for circuit integration, and adaptability for wide working conditions, which have not been systematically investigated yet. In detail, instead of solely pursuing maximum charge storage ability at the electrode/electrolyte interface as for supercapacitors, realizing voltage-/frequency-independent transduction between electronic and ionic signals (high-fidelity electron-ion transduction) is the core target for ionotronics. In another word, a high-performance ionotronic device desires its electronic signal in a

linear and constant relationship with the ionic signal regardless of voltage and frequency, which unfortunately is not the case for current ionotronics at low-frequency input and thus severely limited their functionality and applicability. Meanwhile, they are also required to remain operatable at full-weather conditions in real-life usages (e.g., soft touching, sensing, and low-grade energy harvesting in cold winter), which have not been fulfilled for most hydrogel ionotronics either. Overall, the issues of low ionic conductance, high interfacial impedance, and their poor temperature tolerance all call for an effective new solution to improve the performance of hydrogel ionotronics, specifically the signal fidelity, voltage tolerance, reproducibility, and long-term usage under wide-range frequencies and temperatures.

Here, we propose a strategy to remedy these issues by developing a highly ionically conductive hydrogel to construct ionotronic devices and employing an electrically conductive porous soft polymer (in lieu of metal) as both the electrode and conductor to bridge the ion-based hydrogel ionotronics with the electron-based external circuits. Specifically, the hydrogel was prepared from polyacrylamide (PAAm) as the matrix and  $H_2SO_4$  as the electrolyte through a one-step gelation upon exposure to UV light, thus making it compatible with various fabrication techniques such as templating, mask, and 3D printing methods (Figure 1c). The  $H_2SO_4$  solution provided not only an ultra-high conductivity ( $\approx 70$  S  $m^{-1}$  at 20 °C,  $\approx 6$  S  $m^{-1}$  at  $-60$  °C, and also a pronounced antifreezing capability without introducing an additional antifreezing agent. By contrast, antifreezing hydrogels reported previously usually showed much low conductivities ( $< 1$  S  $cm^{-1}$  at  $-60$  °C), due to the decreased ionization degrees of salts in organic mixture solutions (such as DMSO-based hydrogel) and/or the lower ionic mobility than hydrated  $H^+$  (such as ionic-liquid-based hydrogel).<sup>[17–29]</sup> The hydrogel also demonstrated good stretchability, high transparency, and the ability to be encapsulated by silicone elastomer for high stability and multi-functionality.

A poly(3,4-ethylenedioxythiophene):poly(styrenesulfonate) (PEDOT:PSS) film was employed as a capacitive electrode ( $\approx 19$  F  $cm^{-3}$ ) to replace metal electrodes commonly used

in ionotronics (Figure 1d). This was selected over other conductive porous electrodes (such as porous carbon materials,  $<30 \text{ S cm}^{-1}$ )<sup>[30]</sup> due to its high conductivity ( $750 \text{ S cm}^{-1}$ ) to serve as a conductor to external circuits, easy fabrication, and easy storage in an ambient environment for direct use.<sup>[31]</sup> When attached to an  $\text{H}_2\text{SO}_4$ -based ionic conductor with applied bias, the PEDOT:PSS electrode exhibited a constrained swelling upon  $\text{H}^+$  and  $\text{HSO}_4^-$  migration in its matrix, which facilitated the easy integration of ionotronics with conventional electronics through good Ohmic contact with metal leads. The  $\text{H}_2\text{SO}_4$ -based hydrogel also provided a good acid environment to endow PEDOT:PSS with an ideal EDL capacitance, owing to its unique nature as a mixed ionic-electronic conductor and less doping/dedoping change when in an acid-doped dipole state.<sup>[32–34]</sup> Such a high EDL effectively decreased the interfacial impedance and successfully enabled a stable ion/electron transduction under a wide frequency range of  $0.1\text{--}10^5 \text{ Hz}$ , high voltage tolerance, excellent signal fidelity, and an outstanding low-temperature resistance ability (down to  $-60 \text{ }^\circ\text{C}$ ), substantially outperforming ionotronic counterparts using metal as electrodes.

To demonstrate its promise for applications in soft robotics, energy harvesting, and stretchable devices, here we fabricated two exemplary stretchable, transparent, and antifreezing hydrogel ionotronics: A triboelectric nanogenerator (TENG, silicon rubber as encapsulation layer and electrification layer) showed a much higher output voltage and current than the TENG with only Cu conductor as the deformability of the soft hydrogel. A surface-capacitive touch panel demonstrated its merit of optical transparency for displaying in human-machine-interaction-related applications. Its working frequency was successfully expanded into the low-frequency region (e.g.,  $100 \text{ Hz}$ ), which effectively alleviated the undesirable need for high frequencies ( $10^4 \text{ Hz}$ ) required by Au electrode-based counterparts.

## 2. Results and Discussion

### 2.1. Highly Conductive Antifreezing Hydrogel Conductor

The antifreezing PAAm/ $\text{H}_2\text{SO}_4$  hydrogels were prepared by illuminating the sulfuric acid ( $\text{H}_2\text{SO}_4$ ) solution containing acrylamide monomer, crosslinker, and photo-initiator under UV light for 10 min without the need of additional freezing agents or solvent exchanging procedures, which would impact the shape and micro-structures of the hydrogels. This one-step synthesis method facilitated easy fabrication and its integrability with 2D patterning and 3D printing techniques. Besides these, the PAAm hydrogel showed good stability toward sulfuric acid, which inherited most of the desirable properties and advantages of common conductive hydrogels for ionic electronics, such as good transparency, stretchability, and softness (Figure 2a, 2b). For comparison, polyacrylic acid-based hydrogel turned opaque due to the Hofmeister effect when  $\text{H}_2\text{SO}_4$  solution was employed (Figure S1, Supporting Information).<sup>[35]</sup>

The effect of  $\text{H}_2\text{SO}_4$  concentration on the conductivity and antifreezing performance of hydrogels were studied at different temperatures (Figure 2c). With  $\text{H}_2\text{SO}_4$  concentrations ranging from  $0.53$  to  $3.0 \text{ M}$ , the hydrogels (polymer contents of  $\approx 17\%$ ) showed an increase in conductivities from  $15$  to  $50 \text{ S m}^{-1}$  at

$20 \text{ }^\circ\text{C}$ , which could be attributed to the increased concentrations of mobile ions within the hydrogels. Further increase of  $\text{H}_2\text{SO}_4$  concentration above  $3.0 \text{ M}$  resulted in a slight decrease in conductivity, showing a divergence from the  $\text{H}_2\text{SO}_4$  aqueous solution conductivity trend (Figure S2a, Supporting Information). The small deviation is most likely caused by the molecular interaction between  $\text{H}_2\text{SO}_4$  and PAAm.<sup>[36–38]</sup> Decreasing the temperature led to a corresponding decrease in the hydrogel conductivity. For example, a hydrogel prepared from  $0.53 \text{ M}$   $\text{H}_2\text{SO}_4$  exhibited a 28% decrease in conductivity from  $15.4$  at  $20 \text{ }^\circ\text{C}$  to  $11.2 \text{ S m}^{-1}$  at  $0 \text{ }^\circ\text{C}$ , and to  $2.6 \text{ S m}^{-1}$  with an abrupt increase in relative standard deviation (RSD) at  $-20 \text{ }^\circ\text{C}$  as the uncontrolled formation of solid crystals occurred (Figure 2c, Figure S2b, Supporting Information). Finally, at  $-40 \text{ }^\circ\text{C}$ , the hydrogel was completely frozen as indicated by the unstable and high resistance beyond the measurement range.

By contrast, the hydrogels prepared with  $4.7$  and  $6.2 \text{ M}$   $\text{H}_2\text{SO}_4$  showed excellent antifreezing ability, with conductivities of as high as  $7.6$  and  $8.7 \text{ S m}^{-1}$  at  $-40 \text{ }^\circ\text{C}$ , and  $6.0$  and  $7.7 \text{ S m}^{-1}$  at  $-60 \text{ }^\circ\text{C}$ , respectively (Figure 2b, 2c). Moreover, the conductivity could be further increased by decreasing the polymer contents of hydrogel to enhance ion mobility (Figure 2d). For instance, the hydrogel with a polymer content of 9% showed conductivities of as high as  $70 \text{ S m}^{-1}$  at  $20 \text{ }^\circ\text{C}$  and  $5.7 \text{ S m}^{-1}$  with a small RSD ( $< 0.1$ ) at  $-60 \text{ }^\circ\text{C}$ , which is much higher than the values reported in the previous literature (Figure 2d and Figure S3, Supporting Information). For example, the ionic liquid hydrogel had a low conductivity of only  $1.7 \text{ S m}^{-1}$  at  $-60 \text{ }^\circ\text{C}$ . Therefore, the PAAm/ $\text{H}_2\text{SO}_4$  hydrogel has excellent ionic conductivities, strong antifreezing ability at a temperature as low as  $-60 \text{ }^\circ\text{C}$ , all of which are beneficial for the electrical performance of ionotronics.

Besides good conductivity, all the PAAm/ $\text{H}_2\text{SO}_4$  hydrogels also had good transparency at room temperature (Figure 2b and Figure S4, Supporting Information). Upon decreasing temperature to  $-60 \text{ }^\circ\text{C}$ , hydrogels prepared with  $4.7$  and  $6.2 \text{ M}$   $\text{H}_2\text{SO}_4$  remained highly transparent, enabling the fabrication of transparent electronics at low temperatures. By contrast, the hydrogels prepared with  $0.53 \text{ M}$   $\text{H}_2\text{SO}_4$  turned white at  $-20 \text{ }^\circ\text{C}$  due to the formation of ice crystals, while the hydrogels prepared with  $1.7$  and  $3.0 \text{ M}$   $\text{H}_2\text{SO}_4$  froze at  $-40 \text{ }^\circ\text{C}$  indicating a higher freezing point than the higher concentration hydrogel.

The antifreezing hydrogel inherited the stretchability of common polymer hydrogels at room temperature ( $\approx 20 \text{ }^\circ\text{C}$ ) and was able to be twist and knot at  $-60 \text{ }^\circ\text{C}$ , while the pure PAAm hydrogel exhibited a high rigidity when subjected to similar temperatures and was prone to fracture upon deformation, indicating poor antifreezing performance (Figure 2f). The effect of  $\text{H}_2\text{SO}_4$  concentration on the mechanical properties of hydrogel was first studied (Figure S5, Supporting Information). Compared to the pure PAAm hydrogel without  $\text{H}_2\text{SO}_4$  (fractural strain:  $\approx 470\%$ , Youngs' modulus:  $\approx 22 \text{ kPa}$ ), the hydrogel prepared with  $0.53 \text{ M}$   $\text{H}_2\text{SO}_4$  showed a smaller fractural strain ( $\approx 300\%$ ) with a similar Youngs' modulus ( $\approx 24 \text{ kPa}$ ). The fractural strain increased from  $\approx 300\%$  to  $\approx 450\%$  as the  $\text{H}_2\text{SO}_4$  concentrations increased from  $0.53$  to  $3.0 \text{ M}$ , and then remained stable when the concentration further increased to  $6.2 \text{ M}$ , indicating the good stability of PAAm towards  $\text{H}_2\text{SO}_4$  solutions with a wide range of concentrations. Moreover, the mechanical

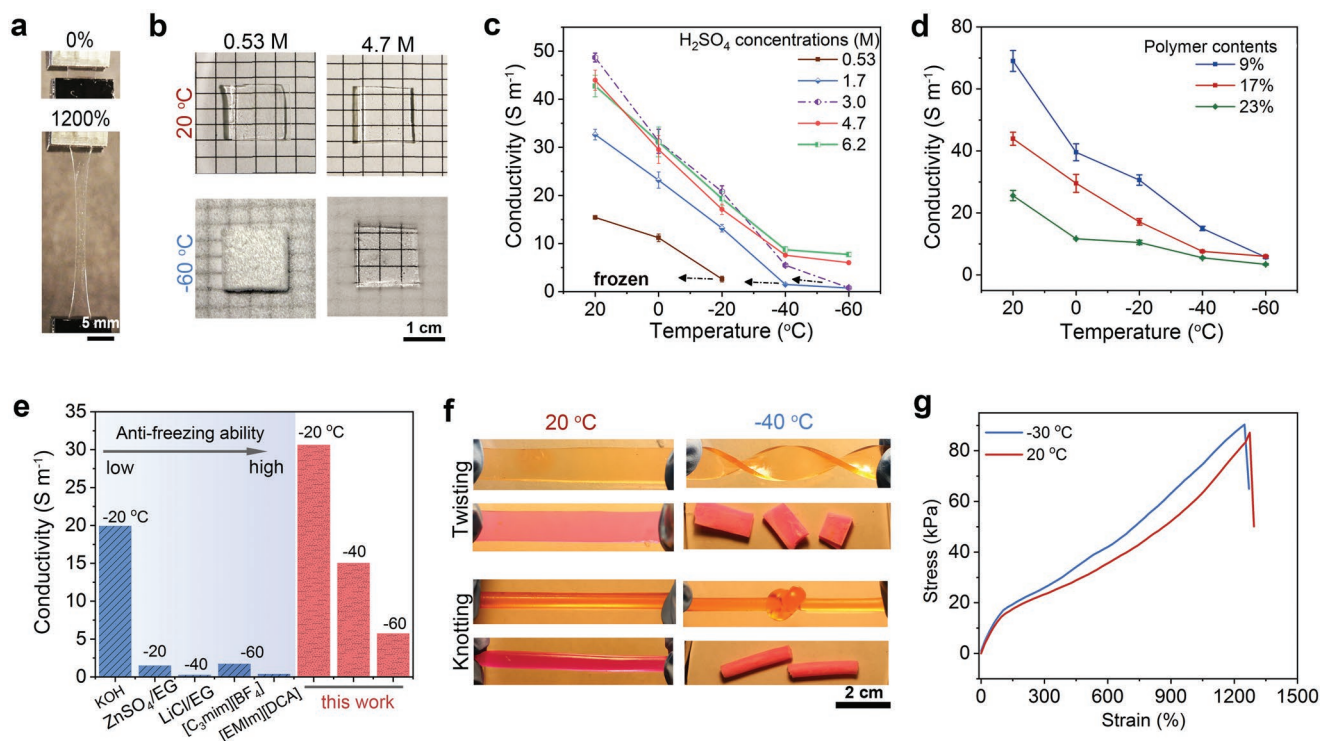


**Figure 2.** Physical properties of PAAm/H<sub>2</sub>SO<sub>4</sub> hydrogels. a) High stretchability shown by the digital photographs of antifreezing PAAm/H<sub>2</sub>SO<sub>4</sub> hydrogels prepared using 4.7 M H<sub>2</sub>SO<sub>4</sub> (ATH<sub>4.7</sub>, crosslinker contents: 0.5% relative to the monomer) before and after stretching. b) Digital photographs of hydrogels (polymer content: 17%) prepared with 0.53 and 4.7 M H<sub>2</sub>SO<sub>4</sub> as precursor solution at 20 and –60 °C, showing the antifreezing ability of the latter. c) Ionic conductivities of PAAm/H<sub>2</sub>SO<sub>4</sub> hydrogel prepared with different concentrations of H<sub>2</sub>SO<sub>4</sub> as precursor solution. d) Ionic conductivity of the ATH<sub>4.7</sub> with different polymer contents. e) Conductivity comparison of ATH<sub>4.7</sub> (polymer content: 9%) with other typical antifreezing hydrogels reported before, including hydrogel infiltrated with KOH, ZnSO<sub>4</sub>/EG, LiCl/EG, and ILs at different temperatures. f) Digital photographs of ATH<sub>4.7</sub> (dye yellow) and common PAAm hydrogel prepared with water as precursor solution (dye pink). The ATH<sub>4.7</sub> could be stretched and twisted at 20 and –30 °C, while the common PAAm hydrogels were frozen and brittle at –30 °C. g) Tensile stress-strain curves of ATH<sub>4.7</sub> with crosslinker contents of 0.5% at 20 or –30 °C

properties were also tunable by changing the crosslinking density and polymer contents, with the fracture strains and Young's modulus in the range of 300%–1250% and 70–3.5 kPa respectively, and could be maintained at low temperatures (Figure 2g, Figures S6 and S7, Supporting Information). Upon decreasing the temperature to –30 °C, all the hydrogels prepared with 4.7 M H<sub>2</sub>SO<sub>4</sub> showed similar mechanical properties with good transparency compared to hydrogels at 20 °C.

## 2.2. Stretchable and Antifreezing Hydrogel-Based TENGs

With the PAAm/H<sub>2</sub>SO<sub>4</sub> hydrogel as the ionic conductor, stretchable, soft, and transparent triboelectric nanogenerators with excellent antifreezing performance were fabricated in a single-electrode configuration by coating the hydrogel with a thin layer of elastomer (EcoFlex 00–30) as the electrification layer. When compared to the conventional electromagnetic generator based on the electrification and induction principle, TENGs could be made stretchable and soft, and could harvest low-frequency mechanical energy efficiently.<sup>[39–43]</sup> In the mechanism (Figure S8, Supporting Information), when a positive triboelectric material (Al foil) contacted the elastomer, the same amounts of charges with opposite polarities were therefore

generated on the interface. Upon the Al foil moving apart, the static charges on the surface of the elastomer could induce a current flowing from the ground via two electric-double layers within the elastomer/hydrogel and hydrogel/electrode interfaces, respectively. Then, the current direction could be reversed to complete one cycle by moving the Al foil back to the elastomer film. Therefore, an AC can be produced by repeating the contact-separation movements.<sup>[44]</sup>

When contacted with the Al foil at a frequency of 0.5 Hz, the open-circuit voltage and short-circuit current of the TENGs were measured. The TENG fabricated with the antifreezing PAAm/H<sub>2</sub>SO<sub>4</sub> hydrogel (prepared with 4.7 M H<sub>2</sub>SO<sub>4</sub>) exhibited a high open-circuit voltage of 16.5 V and a high short-circuit current of 145 nA with good stability for 12000 cycles, which were substantially better than that of Cu-based TENGs (only 4.08 V and 18.5 nA) (Figures S9, S13–S15, Supporting Information). The excellent performance could be attributed to the seamless hydrogel/elastomer interface, thanks to the great softness and deformability of the hydrogel. By varying the loaded resistance, the output power density reached its maximum value of 2.70 mW cm<sup>–2</sup> at 200 MΩ with an energy efficiency of ≈10% (Figures S10–S12, Supporting Information). In addition, the excellent antifreezing ability of the hydrogel enabled the TENG to be functional at low temperatures such as ≈–30 °C,

with an open-circuit voltage of 10.4 V, short-circuit current of 75.3 nA, and a maximum output power density of 200 nW cm<sup>-2</sup> upon a loaded resistor of 400 MΩ (Figure S12, Supporting Information). The moderate ≈50% degradation in the output performance might be ascribed to the lower induction efficiency between elastomer and hydrogel possibly because of the displacement of the elastomer/hydrogel interface. For comparison, the TENG fabricated from PAAm hydrogel with 0.53 M H<sub>2</sub>SO<sub>4</sub> showed a low antifreezing capability, with a significant ≈80% deterioration in open-circuit voltage (0.70 V), short-circuit current of (4.8 nA) at a temperature of -30 °C, as the freezing of hydrogel led to a deformation of the elastomer/hydrogel interface and a constrained ionic movement for the induction (Figure S9, Supporting Information).

### 2.3. Antifreezing Capacitive PEDOT:PSS Electrode and the Interfacial Impedance

Besides the ionic conductivity, the electrode/hydrogel interfacial impedance, an indicator of electron-ion transduction, also strongly affects the overall electrical properties of ionotronics, especially in a low-frequency AC.

In principle, at low-frequency (< 100 Hz), when a low-impedance device is loaded, the electrical properties of ionotronics are usually dominated by the electrode/hydrogel impedance rather than ionic conductance of hydrogel conductor, and the current is expected to increase by increasing the capacitance of the electrode (Equation (1)).<sup>[45]</sup> With a high-impedance device loaded, the current ( $\tilde{I}$ ) flowing through the device is mainly determined by the device, and thus the interfacial voltage ( $\tilde{V}_{\text{int}}$ ) of the hydrogel/electrode has a linear relationship with the interfacial impedance (Equation (2)).

$$\tilde{Z} = \tilde{Z}_{\text{ino}} + \tilde{Z}_{\text{L}} = R_{\text{i}} - \frac{1}{\omega C_{\text{e}}} j + \tilde{Z}_{\text{L}} \cong -\frac{1}{\omega C_{\text{e}}} j \quad (1)$$

$$\tilde{V}_{\text{int}} = \tilde{I} \cdot \frac{1}{\omega C_{\text{e}}} j \quad (2)$$

where  $\tilde{Z}$  is the overall impedance consists of the impedance of hydrogel ionotronics ( $\tilde{Z}_{\text{ino}}$ ) and loaded devices ( $\tilde{Z}_{\text{L}}$ ),  $R_{\text{i}}$ ,  $\omega$ , and  $C_{\text{e}}$  are the ionic resistance of hydrogel, angular frequency of AC, and the capacitance of electrode, respectively.

To reveal the impact of interfacial impedance in experiments, a pair of Au electrodes were used to connect with the two ends of a PAAm/H<sub>2</sub>SO<sub>4</sub> ionic conductor (Figure 3a and Figure S16, Supporting Information), and the electrical behavior of the Au-based ionotronics (Au-IC) was studied by electrochemical impedance spectra (EIS) and AC amperometric curves. According to the Bode plots in the EIS with an amplitude of 0.1 V, the Au-IC showed a low impedance of ≈24.5 Ω with a phase angle of 1.8° at a high frequency of 10<sup>5</sup> Hz. These behaviors mainly reflected the electrolyte resistance of the hydrogel, as the interfacial impedance was almost negligible as indicated by the ≈ 0° phase angle at this frequency (Figure 3c). However, as the frequency decreased, the overall electrical response of the ionotronics became gradually dominated by the high electrode/hydrogel interfacial impedance, showing a nearly 125-time

increase, up to 30.6 kΩ at 0.1 Hz. Moreover, the Au-IC exhibited an unstable phase angle with an obvious shoulder peak at ≈100 Hz (Figure 3d), revealing that electrochemical side-reactions occurred on the Au electrodes. This faradic process was intensified upon a relatively high AC amplitude such as 0.6 V, as shown by the significantly decreased phase angle from 70.3° to 38.6° at 0.1 Hz indicating an activated electrochemical reaction upon the application of high voltage. The unstable and high interfacial impedances were further proved by AC amperograms where a sinusoid AC voltage was applied to the Au-IC (Figure 3e). The recorded currents flowing through the Au-IC over time showed significant distortion from standard sinusoid curves even upon an AC voltage with a lower amplitude of 0.1 V (Figure S17, Supporting Information). Moreover, this deviation became more severe with the amplitude increased from 0.1 to 0.6 V, consistent with the voltage-dependent impedance as shown in the EIS (Figure 3c, 3d). Overall, even by using the inert metal Au as the electrode, the hydrogel-based ionotronics still showed an unstable electrical behavior, influenced strongly by the AC frequency and amplitude. These issues are mainly ascribed to the high interfacial impedance and uncontrollable electrochemical reaction on the electrode, severely impacting the interfacial stability and complicating the electronic-ionic transduction and signal processing in low-frequency-related applications.

To solve these issues, a highly conductive and capacitive PEDOT:PSS electrode with a thickness of ≈2.5 μm was prepared by drying a DMSO-treated PEDOT:PSS suspension on a polyethylene terephthalate (PET) film (Figure 3b).<sup>[32–34]</sup> The PEDOT:PSS electrode had good conductivity of 750 S cm<sup>-1</sup> and a nearly ideal capacitive behavior when in H<sub>2</sub>SO<sub>4</sub> electrolytes, without significant redox peaks as shown by the quasi-rectangular shape in cyclic voltammogram (CV) curves (Figure 3h). Here, the H<sup>+</sup> in electrolyte provided an acidic environment to stabilize the PEDOT:PSS in a highly conductive bipolaron state with less doping/de-doping change for the formation of an ideal EDL, and boosted the capacitance through more efficient ion adsorption owing to its smaller hydrated ion radius and higher mobility via the jumping transference between water molecules through hydrogen bonds, when compared with other positive ions such as Li<sup>+</sup>, Na<sup>+</sup>, and K<sup>+</sup>.<sup>[31,46,47]</sup> After CV measurement, the PEDOT:PSS electrode could still attach to the PET substrate firmly, indicating its excellent stability, although its thickness increased to ≈6.3 μm with a porous laminar structure, as the result of the electrowetting effect where solid/liquid interfacial tension increased through the EDL formation under the applied voltages (Figure S18, Supporting Information). Based on the expanded thickness, the volumetric capacitance of PEDOT:PSS electrode was calculated to be ≈19 F cm<sup>-3</sup> (Figure S19, Supporting Information). Increasing the concentration of H<sub>2</sub>SO<sub>4</sub> solution from 0.53 to 6.2 M effectively led to an increased capacitance especially at high current density and a decreased equivalent serial resistance, attributed to the decreased Debye length of EDL, low ionic diffusion resistance, and high electrolyte conductivity (S19–S21, Supporting Information).<sup>[48–50]</sup> The capacitive PEDOT:PSS electrodes also showed excellent antifreezing performance with a tolerance temperature of as low as -60 °C (Figure 3h). Upon temperature decreasing, the PEDOT:PSS electrode showed a slight decrease in capacitance from

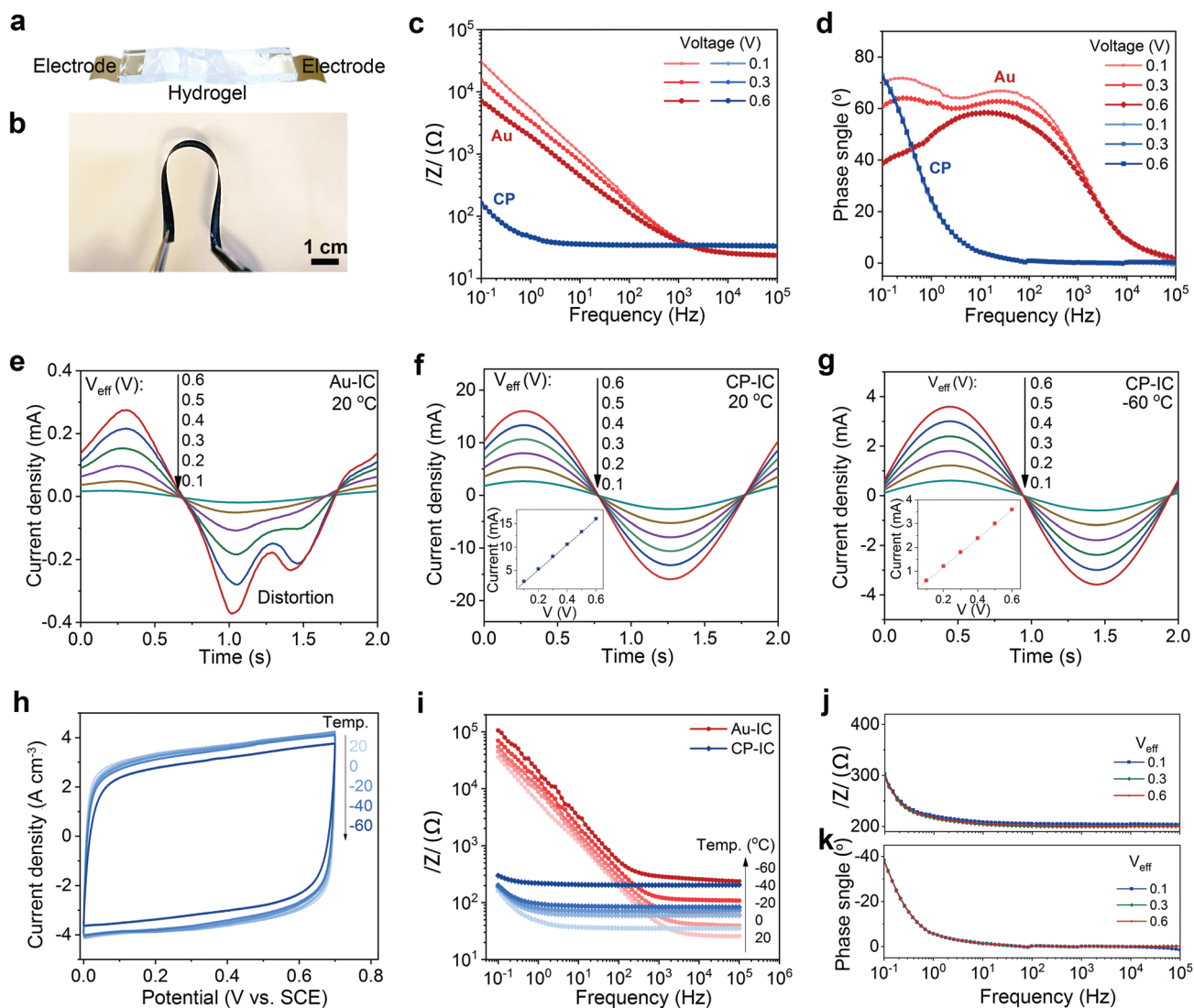


**Figure 3.** Electrical properties of ionotronics. a) Schematics of hydrogel-based ionotronics, where an ionically conductive hydrogel was connected to an external circuit through two electrodes. b) Digital photography of PEDOT:PSS electrode. c,d) Plots of impedance (c) and phase angle (d) versus frequency of Au-IC and CP-IC at 20 °C. e–g) Current–time curves of Au-IC (e) and CP-IC (f, g) upon an AC voltage with an amplitude of 0.1–0.6 V and a frequency of 0.5 Hz at 20 (e, f) or –60 °C (g). h) CVs of PEDOT:PSS electrode in 4.7 m H<sub>2</sub>SO<sub>4</sub> electrolyte at the scan rate of 200 mV s<sup>-1</sup> in the three-electrode configuration. i) Plots of impedance versus frequency of Au-IC and CP-IC at the different temperatures with an amplitude of 5 mV. j,k) Plots of impedance (j) and phase angle (k) versus frequency of CP-IC upon different amplitudes of 0.1–0.6 V at –60 °C.

≈19 to ≈16 F cm<sup>-3</sup>, possibly resulting from the increased electrolyte resistance and slow charge-transfer at low temperature as revealed by EIS (Figures S22–S27, Supporting Information). Though, the PEDOT:PSS electrode still showed double-electric-layered capacitive behavior especially at the lower frequency, with quasi-rectangular CVs and nearly vertical Nyquist plots in EIS spectra (Figures S22–S27, Supporting Information).

The obtained PEDOT:PSS electrode could be stored in an ambient environment without the need for soaking in the electrolyte, and ready for direct use, thus showing its great convenience for connecting hydrogel-based ionic circuits with electronic circuits to construct ion–electron coupled circuits. With the PEDOT:PSS as electrodes, the conducting-polymer-based ionotronics (CP-IC) showed a significantly decreased

impedance at low frequencies, nearly 1000 times lower than the values of Au-IC and Au nanomesh reported previously<sup>[51]</sup> upon the low-frequency region (< 100 Hz), which was attributed to the larger capacitance of the PEDOT:PSS compared to the Au electrodes (Figure 3c). Furthermore, according to the EIS and AC amperograms, the CP-IC showed a much more stable phase angle regardless of input voltage in the ranges of 0–0.6 V with an ideal sinusoid current waveforms in stark contrast with Au-IC, indicating the excellent and stable electrical properties of PEDOT:PSS electrodes for ionotronics (Figure 3d, 3f). Moreover, thanks to the excellent antifreezing capacitive performance of PEDOT:PSS electrode and PAAm/H<sub>2</sub>SO<sub>4</sub> hydrogel, the CP-IC exhibited stable low impedance at low temperature down to –60 °C, independent of the input voltage in the

ranges of 0–0.6 V (Figure 3i–k). In detail, at high AC frequency ( $10^5$  Hz), the impedance of CP-IC increased gradually with a decrease in temperature as the ionic resistance of hydrogel increased. At low frequency, the overall impedance was mainly determined by the electrode/hydrogel interfacial impedance, which could be represented by imaginary impedance, and showed almost no obvious changes (such as 1 Hz) with temperature (Figures S28 and S29, Supporting Information), indicating the stable areal capacitance of PEDOT:PSS electrode at low temperatures. By contrast, at low temperatures, the impedance of Au-IC was still very high and closely related with the input voltages, severely complicating the ion-electron signal transduction and processing of ionotronics and compromising signal fidelity (Figure S29, Supporting Information).

#### 2.4. Antifreezing and Stretchable Touch Panel Working at Low-Frequency AC

To demonstrate the great advantages of PEDOT:PSS over inert metals as electrodes in the antifreezing ionotronics, a hydrogel-based touch panel was fabricated based on the surface-capacitive principle (Figure 4a). As a proof of the concept, the touch panel contains a simple structure, only one hydrogel-based ionic conductor and four electrodes for 2D touch location. Multipoint touch may be further realized by using more electrodes. Unlike the conventional rigid touch panels made of indium tin oxide, the hydrogel-based ionic touch panel is soft, transparent, and stretchable. By employing PEDOT:PSS as electrodes, the ionic touch panel can operate under an AC of low

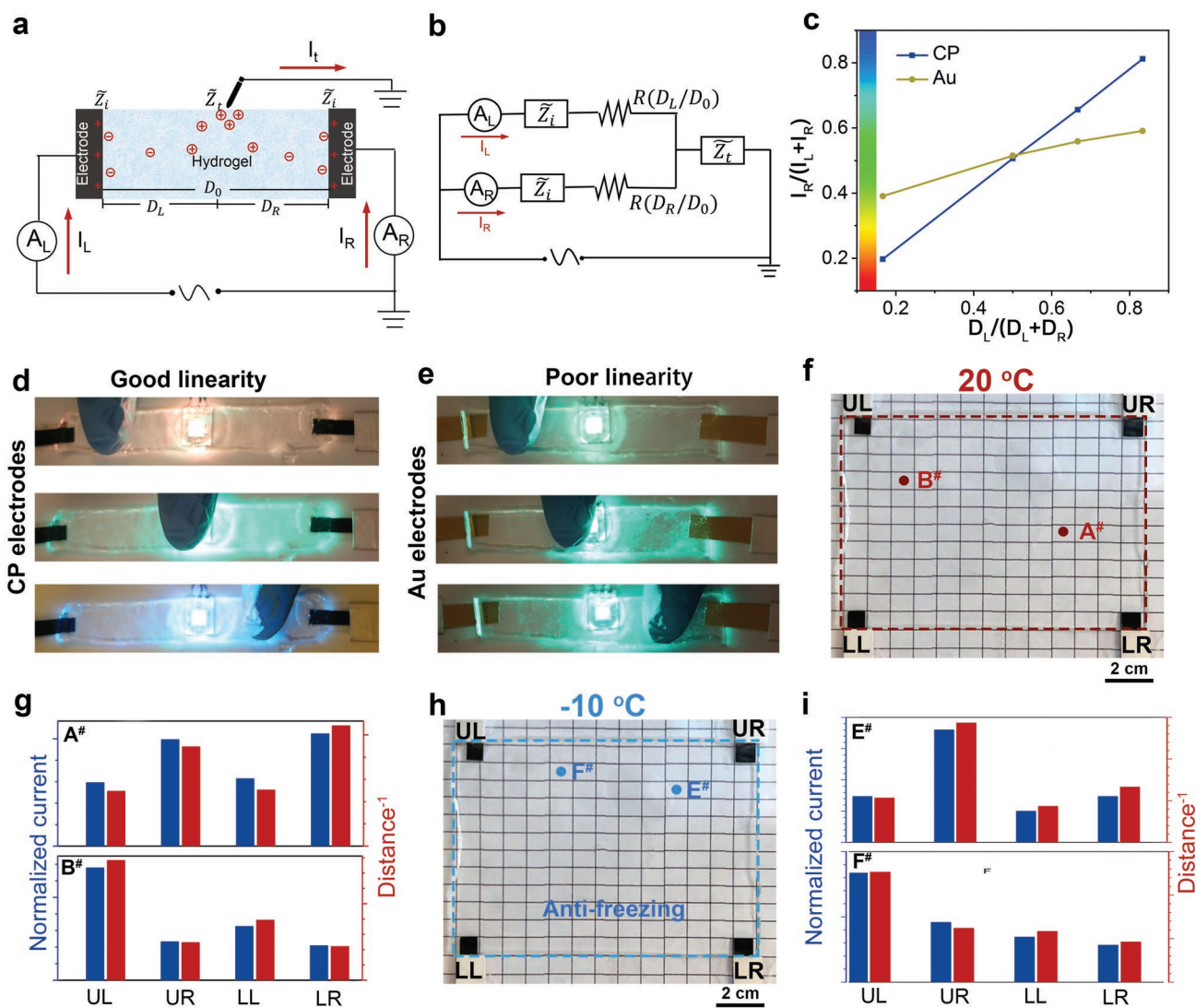


**Figure 4.** Performance of touch panels. a) Schematics of the 1D hydrogel touch panel and the mechanism. b) Equivalent circuit of 1D touch panel. c) Plots of current ratio ( $I_R/I_L$ ) versus proximity of touchpoint to the two electrodes by using CP or Au as electrodes. d,e) Digital photographs of 1D touch panel with CP (d) or Au (e) as electrodes. The color (from red to blue) of the LED beneath the touch panel is controlled by a computer to visualize the touch position (from the left to the right) calculated through the current ratio. f,h) Digital photography of 2D touch panel, where four CP electrodes were attached to the four corners of the hydrogel (UL: upper left, UR: upper right, LL: lower left, LR: lower right). Two arbitrary touchpoints for the experiment at the temperatures of 20 °C (f,  $A^\#$  and  $B^\#$ ) or -10 °C (h,  $E^\#$  and  $F^\#$ ) were marked respectively. g,i) Normalized current through the four CP electrodes when the points shown in the panels f and h, respectively were touched by a grounded finger as a conductor.

frequency (such as 100 Hz), which successfully alleviated the reliance on high-frequency AC ( $10^4$  Hz) required by conventional ionotronics, and thus simplified the whole circuit when integrated with other devices.

First, by using Au or PEDOT:PSS as electrodes, their performance in touch panels was compared by using a 1D touch strip (Figure 4c). In detail, a strip of PAAm/ $H_2SO_4$  hydrogel was connected to a pair of PEDOT:PSS electrodes with the same phase AC voltage applied at a frequency of 100 Hz. Without being touched, the whole device was nearly open-circuited. When the hydrogel strip was touched by a grounding electrode, the currents were flowing through the circuit via the interfacial capacitor produced between conductor and hydrogel. For detailed mechanism, the equivalent circuit of the ionic device is shown in Figure 4b, where  $Z_i$  and  $Z_t$  represent the interfacial impedances of electrode/hydrogel and touch-pen/hydrogel, and  $R_L$  and  $R_R$  represent the ionic resistance of hydrogel, linearly relating with the proximity of touchpoint to the left and right electrodes. Since PEDOT:PSS electrodes exhibit an extraordinarily stable and low impedance, as proven earlier in this work, the  $Z_i$  in the equivalent circuit was almost negligible. Therefore, the current ratio  $\left(\frac{I_R}{I_R + I_L}\right)$  was determined by the ionic resistance ratio  $\left(\frac{R_L}{R_L + R_R}\right)$  and thus determined by the proximity of the touching point to the two electrodes at the ends of strips  $\left(\frac{D_L}{D_L + D_R}\right)$ . For the PEDOT:PSS electrodes, the current ratio demonstrated a clear linear relationship with the proximity ratio ranging from 0.2 to 5 (Figure 4c, d). For comparison, for the Au-based touch panel, the relationship was nonlinear, as the high and unstable electrode/hydrogel impedance invalidated the devices under low-frequency AC (Figure 4c, e).

Then, a 2D touch panel was fabricated with a similar configuration but including four PEDOT:PSS electrodes one for on each corner of the hydrogel (Figure S6f, Supporting Information). Similar to the trend for the 1D touch strip, the 2D touch panel also displayed a proximity-dependent current through the four electrodes. Four touch points (A<sup>#</sup>, B<sup>#</sup>, C<sup>#</sup>, and D<sup>#</sup>) were detected to clarify the relationship of the current ratio with the relative distance to electrodes (Figures S6g and S30, Supporting Information). For example, when point A<sup>#</sup> was touched, the electrode UR had the highest current, and the electrode LL had the least. At last, the touch panel could also operate at a low temperature of  $-10$  °C as an example, where the current ratio also showed a quasi-inverse relationship with the proximity of the touchpoint to the electrodes (Figures S6h, S6i and S31, Supporting Information). Though application at lower temperature was not demonstrated, the device developed here is expected to well function at a temperature down to  $-60$  °C, according to the impedance results of the antifreezing PEDOT:PSS electrode shown above.

### 3. Conclusion

To improve the overall electrical response of ionotronics across a wide AC frequency and temperature range, a strategy of combing antifreezing highly conductive hydrogels

(PAAm/ $H_2SO_4$ ) with quasi-solid porous and conductive PEDOT:PSS electrodes was proposed. The  $H_2SO_4$  used in the hydrogel has four roles here, including i) improving the ionic conductivity, ii) expanding the working temperature down to  $-60$  °C, iii) enhancing the electrical-double-layered capacitance of PEDOT:PSS electrode as the smaller hydrated ion radius and high mobility of  $H^+$ , iv) stabilizing the redox state and thus electrical properties of the highly conductive and capacitive PEDOT:PSS electrodes through acid doping. The hydrogel exhibited an ultra-high conductivity across a wide temperature range ( $\approx 70$  S  $m^{-1}$  at 20 °C,  $\approx 6$  S  $cm^{-1}$  at  $-60$  °C), benefiting the electrical performance especially at a high-frequency AC. The hydrogel was transparent, stretchable, and could be easily prepared by one-step photo-induced gelation. Besides a high ionic conductance, a stable and efficient ion/electron transduction was also realized which dominated the electrical performance of hydrogel ionotronics, as shown by a much low interfacial impedance under AC of 0.1– $10^5$  Hz, high voltage tolerance, excellent signal fidelity, and an outstanding low-temperature resistance ability (down to  $-60$  °C), substantially outperforming ionotronic counterparts using metal as electrodes.

As a proof of concept, an antifreezing stretchable TENG and touch panel were fabricated: i) the TENG made from silicon-rubber-encapsulated hydrogel provided a higher output voltage and current than with those with metal as electrodes, attributed to the enhanced softness and deformability of the hydrogel-based TENGs; ii) the ionic touch panel could operate at a much lower frequency (e.g., 100 Hz without the limit of high-frequency current ( $10^4$  Hz) common in hydrogel ionic touch panels with Au as electrodes, given the low and stable impedance of the PEDOT:PSS/hydrogel interface at low temperatures. Besides the excellent electrical performance, the hydrogel ionotronics also showed good transparency, stretchability, and conformability, showing great promise in the integration of various hydrogel-ionotronic units

### 4. Experimental Section

**Preparations of PAAm/ $H_2SO_4$  Hydrogels:** Typically, acrylic amide (20 wt.%, relative to solution), N,N'-methylenebis(acrylamide) (Bis) (2.5 wt.%, relative to monomer), and 2-hydroxy-2-methylpropiophenone ( $2.5 \times 10^{-5}$  wt.%, relative to monomer) as photoinitiator were dissolved in a 4.7 M  $H_2SO_4$  solution. The prepared precursor solution was degassed, poured into a mold, and then was exposed to UV light (Bluewave 200, Dymax) for 10 min to complete the gelation process. For the preparation of hydrogels with different crosslinking densities, polymer contents, and electrolyte concentrations, all the synthetic procedures were the same as above except where noted. In detail, for the preparation of PAAm/ $H_2SO_4$  hydrogels with different crosslinking densities, the Bis' concentrations were altered from 0.1 wt.% to 0.5 wt.%, relative to the monomer. For the preparation of hydrogels with different polymer contents, the content of acrylic amide was tuned in the range of 10–30 wt.%, relative to the solution. For the hydrogel prepared with  $H_2SO_4$  solution of different concentrations, 3.0, 4.7, and 6.2 M  $H_2SO_4$  solution was used, respectively.

**Encapsulation of Hydrogel with EcoFlex:** PAAm/ $H_2SO_4$  hydrogel was immersed in the liquid precursor of EcoFlex which was mixed, degassed, and kept at room temperature for 30 min. Then, the composite was taken out and kept at room temperature for 2 h to cure the Ecoflex (Movie S1, Supporting Information).

**Fabrication of TENG:** PAAm/ $H_2SO_4$  hydrogels (1  $cm^2$ ) were attached with copper wires for electrical connection and then coated with a thin

layer of the dielectric layer by drop-casting Ecoflex 00–30 which was then cured at room temperature for 4 h.

**Preparation of PEDOT:PSS Electrodes:** Commercially available PEDOT:PSS suspensions ( $\approx 13 \text{ mg mL}^{-1}$ , Celvios PH1000, Heraeus) was added with 5 wt. % (relative to the PEDOT:PSS solution) of DMSO, and were kept stirring overnight to induce the phase separation of PEDOT:PSS chains according to the previous literature. Then, the resultant suspension was drop-casted onto PET films ( $\approx 35 \text{ uL per cm}^2$ ) previously treated by  $\text{O}_2$  plasma (PDC-001, Harrick Plasma) for 20 min and dried at  $60^\circ\text{C}$  for 2 h.

**Fabrication of Touch Panel:** For the 1D touch strip, a PAAm/ $\text{H}_2\text{SO}_4$  hydrogel (prepared with  $4.7 \text{ M H}_2\text{SO}_4$ ) with a size of  $75 \text{ mm} \times 5 \text{ mm} \times 2 \text{ mm}$  (length  $\times$  width  $\times$  height) was used as the ionic conductor, either a pair of Au electrodes prepared by sputtering or PEDOT:PSS electrodes were attached on to the two ends of the hydrogels, and then connected to two current meters. The same phase AC voltage with an amplitude of 1 V was applied to the two electrodes simultaneously. For the 2D touch panel, a PAAm/ $\text{H}_2\text{SO}_4$  hydrogel (prepared with  $4.7 \text{ M H}_2\text{SO}_4$ ) with a size of  $65 \text{ mm} \times 48 \text{ mm} \times 2 \text{ mm}$  (length  $\times$  width  $\times$  height) and four PEDOT:PSS electrodes were employed.

**Conductivity and Thickness Measurements of the Hydrogel:** The conductivities of hydrogels at different temperatures were measured through two-electrode configurations. The hydrogels were put in plastic sealed bags and then immersed in a cooling bath of different temperatures (PSL-1810, Eyela). The two ends of hydrogel (width: 0.5 cm, Length: 5.5 cm, Height: 0.1 cm) were connected to an electrical working station (660E, CH instruments) through two Au electrodes ( $0.5 \text{ cm} \times 0.2 \text{ cm}$ ). The conductivities ( $\sigma$ ) were measured by EIS spectra at an initial voltage of 0 V with 5 mV amplitude and frequency of  $10^4 \text{ Hz}$ , and were calculated according to the following equations:

$$\sigma = \frac{l}{R \times w \times d} \quad (3)$$

where  $R$  is the measured resistance.  $l$ ,  $w$ , and  $d$  represent the length, width, and thickness of the hydrogels. The thickness was obtained by a surface profiler (NT9300 Optical Profiler, Bruker).

**Mechanical Testing of Hydrogels:** The PAAm/ $\text{H}_2\text{SO}_4$  hydrogels with a thickness of 1 mm were cut into a rectangle shape with a width of 7.0 mm, and the tensile strain-stress curves were recorded on a mechanical testing system (Univert, CellScale) at a rate of 20% strain per second (gauge length = 2 mm). For the mechanical testing at  $-30^\circ\text{C}$ , the testing environment was cooled down by a cooling system.

**Electrical Measurement of TENG:** The TENGs were fixed at a bottom stage and were repeatedly contacted with an Al foil through a step motor at the frequency of 0.5 Hz, the maximum speed of  $1 \text{ m s}^{-1}$  with an acceleration of  $1 \text{ m s}^{-2}$ . The voltage and the current were measured by a high-impedance electrometer (Keysight, 6514) and a current meter with a preamplifier (Stanford Research System, SR570).

**Electrochemical Measurements of PEDOT:PSS Electrodes:** A three-electrodes configuration was employed to study the electrochemical properties of the PEDOT:PSS electrodes through an electrochemical working station (CHI660E, CH Instrument). PEDOT:PSS electrodes ( $5.5 \text{ cm}^2$ ), Pd/Au plate ( $3 \times 1 \text{ cm}^2$ ), SCE were employed as working, counter, and reference electrodes, respectively.  $4.7 \text{ M H}_2\text{SO}_4$  solution was employed as an electrolyte. CV curves were recorded at a scan rate of  $50\text{--}200 \text{ mV s}^{-1}$  with an electrochemical window of  $0\text{--}0.7 \text{ V}$  (vs  $\text{Hg}/\text{Hg}_2\text{Cl}_2$ ). EIS spectra were obtained at an initial potential of 0 V (vs SCE) with 5 mV amplitude in the frequency range of  $10^5\text{--}0.1 \text{ Hz}$ . The capacitances ( $C$ ) and IR drops ( $U_{IR}$ ) were calculated by galvanostatic curves with the potential window of  $0\text{--}0.7 \text{ V}$  at different cathodic and anodic currents according to the equations:

$$C = \frac{It}{U_a V} \quad (4)$$

$$U_{IR} = 0.7 - U_a \quad (5)$$

where  $I$  is the anodic current,  $t$  is the anodic time,  $U_a$  is the potential at the beginning of the anodic process, and  $V$  is the volume of PEDOT:PSS electrode. After electrical measurement, the thickness of the PEDOT:PSS electrodes was measured by a surface profiler to get the volume.

**Electrochemical Measurements of Au-IC and CP-IC:** A PAAm/ $\text{H}_2\text{SO}_4$  hydrogel (prepared with  $4.7 \text{ M H}_2\text{SO}_4$ ) with a size of 2 mm in thickness, 2.5 cm in width, and 3.7 cm in length was used as the ionic conductor. A pair of Au electrodes prepared by sputtering or PEDOT:PSS electrodes (the active area that contact hydrogel was  $5 \text{ mm} \times 2.5 \text{ cm}$ ) was used as the electrode, which was then connected to an electrochemical working station (660E, CH instruments) (Figure S8, Supporting Information). EIS was recorded at an initial voltage of 0 V and frequency of  $0.1\text{--}10^5 \text{ Hz}$  with different amplitudes. AC amperometric curves were obtained at an initial voltage of 0 V and frequency of 0.5 Hz.

## Supporting Information

Supporting Information is available from the Wiley Online Library or from the author.

## Acknowledgements

X.H. acknowledges NSF CAREER award 1724526, AFOSR awards FA9550-17-1-0311, FA9550-18-1-0449, and FA9550-20-1-0344, and ONR awards N000141712117 and N00014-18-1-2314.

## Conflict of Interest

The authors declare no conflict of interest.

## Data Availability Statement

The data that supports the findings of this study are available in the supplementary material of this article.

## Keywords

antifreezing hydrogels, impedance, ion-electron transduction, ionic devices

Received: October 21, 2021

Published online:

- [1] Y. Zou, P. Tan, B. Shi, H. Ouyang, D. Jiang, Z. Liu, H. Li, M. Yu, C. Wang, X. Qu, L. Zhao, Y. Fan, Z. L. Wang, Z. Li, *Nat. Commun.* **2019**, *10*, 2695.
- [2] J. Park, S. Heo, K. Park, M. H. Song, J. Y. Kim, G. Kyung, R. S. Ruoff, J. U. Park, F. Bien, *npj Flex. Electron.* **2017**, *1*, 9.
- [3] J. H. Kim, J. W. Park, *Sci. Adv.* **2021**, *7*, eabd9715.
- [4] T. Chen, Q. Shi, M. Zhu, T. He, L. Sun, L. Yang, C. Lee, *ACS Nano* **2018**, *12*, 11561.
- [5] Y. Zhao, C. Y. Lo, L. Ruan, C. H. Pi, C. Kim, Y. Alsaied, I. Frenkel, R. Rico, T. C. Tsao, X. He, *Sci. Robot.* **2021**, *6*, eabd5483.
- [6] M. Cianchetti, C. Laschi, A. Menciassi, P. Dario, *Nat. Rev. Mater.* **2018**, *3*, 143.
- [7] C. Yang, Z. Suo, *Nat. Rev. Mater.* **2018**, *3*, 125.
- [8] X. Liu, J. Liu, S. Lin, X. Zhao, *Mater. Today* **2020**, *36*, 102.
- [9] H. J. Kim, B. H. Chen, Z. Suo, R. C. Hayward, *Science* **2020**, *367*, 773.

- [10] C. Keplinger, J. Y. Sun, C. C. Foo, P. Rothemund, G. M. Whitesides, Z. Suo, *Science* **2013**, *341*, 984.
- [11] X. Pu, M. M. Liu, X. Y. Chen, J. M. Sun, C. H. Du, Y. Zhang, J. Y. Zhai, W. G. Hu, Z. L. Wang, *Sci. Adv.* **2017**, *3*, e1700015.
- [12] Q. Guan, G. Lin, Y. Gong, J. Wang, W. Tan, D. Bao, Y. Liu, Z. You, X. Sun, Z. Wen, Y. Pan, *J. Mater. Chem. A* **2019**, *7*, 13948.
- [13] T. B. H. Schroeder, A. Guha, A. Lamoureux, G. VanRenterghem, D. Sept, M. Shtein, J. Yang, M. Mayer, *Nature* **2017**, *552*, 214.
- [14] B. Kim, J. Na, H. Lim, Y. Kim, J. Kim, E. Kim, *Adv. Funct. Mater.* **2019**, *29*, 1807549.
- [15] C. H. Yang, B. Chen, J. Zhou, Y. M. Chen, Z. Suo, *Adv. Mater.* **2016**, *28*, 4480.
- [16] C. C. Kim, H. H. Lee, K. H. Oh, J. Y. Sun, *Science* **2016**, *353*, 682.
- [17] D. Bao, Z. Wen, J. Shi, L. Xie, H. Jjiang, J. Jjiang, Y. Yang, W. Liao, X. Sun, *J. Mater. Chem. A* **2020**, *8*, 13787.
- [18] X. P. Morelle, W. R. Illeperuma, K. Tian, R. Bai, Z. Suo, J. J. Vlassak, *Adv. Mater.* **2018**, *30*, 1801541.
- [19] X. F. Zhang, X. Ma, T. Hou, K. Guo, J. Yin, Z. Wang, L. Shu, M. He, J. Yao, *Angew. Chem., Int. Ed.* **2019**, *58*, 7366.
- [20] Q. Rong, W. Lei, J. Huang, M. Liu, *Adv. Energy Mater.* **2018**, *8*, 1801967.
- [21] M. Ju, B. Wu, S. Sun, P. Wu, *Adv. Funct. Mater.* **2020**, *30*, 1910387.
- [22] X. T. Jin, G. Q. Sun, G. F. Zhang, H. S. Yang, Y. K. Xiao, J. Gao, Z. P. Zhang, L. T. Qu, *Nano Res.* **2019**, *12*, 1199.
- [23] Y. Ding, J. Zhang, L. Chang, X. Zhang, H. Liu, L. Jjiang, *Adv. Mater.* **2017**, *29*, 1704253.
- [24] Z. Cao, H. Liu, L. Jjiang, *Mater. Horiz.* **2020**, *7*, 912.
- [25] Y. Ren, J. Guo, Z. Liu, Z. Sun, Y. Wu, L. Liu, F. Yan, *Sci. Adv.* **2019**, *5*, eaax0648.
- [26] Z. Pei, Z. Yuan, C. Wang, S. Zhao, J. Fei, L. Wei, J. Chen, C. Wang, R. Qi, Z. Liu, Y. Chen, *Angew. Chem., Int. Ed.* **2020**, *59*, 4793.
- [27] S. Wu, Y. Alsaïd, B. Yao, Y. Yan, Y. Zhao, M. Hua, D. Wu, X. Zhu, X. He, *EcoMat* **2021**, *3*, e12085.
- [28] X. Jin, L. Song, H. Yang, C. Dai, Y. Xiao, X. Zhang, Y. Han, C. Bai, B. Lu, Q. Liu, Y. Zhao, J. Zhang, Z. Zhang, L. Qu, *Energy Environ. Sci.* **2021**, *14*, 3075.
- [29] T. Xu, D. Yang, S. Zhang, T. Zhao, M. Zhang, Z.-Z. Yu, *Carbon* **2021**, *171*, 201.
- [30] X. Yang, C. Cheng, Y. Wang, L. Qiu, D. Li, *Science* **2013**, *341*, 534.
- [31] B. D. Paulsen, K. Tybrandt, E. Stavrinidou, J. Rivnay, *Nat. Mater.* **2020**, *19*, 13.
- [32] J. Y. Kim, J. H. Jung, D. E. Lee, J. Joo, *Synth. Met.* **2002**, *126*, 311.
- [33] L. V. Lingstedt, M. Ghittorelli, H. Lu, D. A. Koutsouras, T. Marszalek, F. Torricelli, N. I. Crăciun, P. Gkoupidenis, P. W. M. Blom, *Adv. Electron. Mater.* **2019**, *5*, 1800804.
- [34] B. Y. Lu, H. Yuk, S. T. Lin, N. N. Jian, K. Qu, J. K. Xu, X. H. Zhao, *Nat. Commun.* **2019**, *10*, 1043.
- [35] A. Sinek, M. Kupczak, A. Mielanczyk, M. Lemanowicz, S. Yusa, D. Neugebauer, A. Gierczycki, *Polymers* **2020**, *12*, 486.
- [36] B. Y. Xiong, R. D. Loss, D. Shields, T. Pawlik, R. Hochreiter, A. L. Zydny, M. Kumar, *npj Clean Water* **2018**, *1*, 17.
- [37] Y. D. Livney, I. Portnaya, B. Faupin, O. Ramon, Y. Cohen, U. Cogan, S. Mizrahi, *J. Polym. Sci., Part B: Polym. Phys.* **2003**, *41*, 508.
- [38] H. Li, A. Erbaş, J. Zwanikken, M. Olvera de la Cruz, *Macromolecules* **2016**, *49*, 9239.
- [39] F. R. Fan, Z. Q. Tian, Z. L. Wang, *Nano Energy* **2012**, *1*, 328.
- [40] F. R. Fan, W. Tang, Y. Yao, J. Luo, C. Zhang, Z. L. Wang, *Nanotechnology* **2014**, *25*, 135402.
- [41] C. Zhang, W. Tang, C. Han, F. Fan, Z. L. Wang, *Adv. Mater.* **2014**, *26*, 3580.
- [42] A. Ahmed, I. Hassan, A. S. Helal, V. Sencadas, A. Radhi, C. K. Jeong, M. F. El Kady, *Iscience* **2020**, *23*, 101286.
- [43] J. Peng, S. D. Kang, G. J. Snyder, *Sci. Adv.* **2017**, *3*, eaap8576.
- [44] R. Wang, L. Mu, Y. Bao, H. Lin, T. Ji, Y. Shi, J. Zhu, W. Wu, *Adv. Mater.* **2020**, *32*, 2002878.
- [45] M. Itagaki, S. Suzuki, I. Shitanda, K. Watanabe, *Electrochemistry* **2007**, *75*, 649.
- [46] B. Pal, S. Y. Yang, S. Ramesh, V. Thangadurai, R. Jose, *Nanoscale Adv.* **2019**, *1*, 3807.
- [47] M. Berggren, G. G. Malliaras, *Science* **2019**, *364*, 233.
- [48] J. P. Zheng, T. R. Jow, *J. Electrochem. Soc.* **1997**, *144*, 2417.
- [49] C. Prehal, C. Koczwara, H. Amenitsch, V. Presser, O. Paris, *Nat. Commun.* **2018**, *9*, 4145.
- [50] W. C. Johnson, P. T. Panousis, *IEEE Trans. Electron Devices* **1971**, *18*, 965.
- [51] W. L. Li, N. Matsuhisa, Z. Y. Liu, M. Wang, Y. F. Luo, P. Q. Cai, G. Chen, F. L. Zhang, C. C. Li, Z. H. Liu, Z. S. Lv, W. Zhang, X. D. Chen, *Nat. Electron.* **2021**, *4*, 134.